5-2014

Neutron Imaging of Lithium (Li) Coolants inside High Temperature Niobium (Nb) Heat Pipes

Brad Harrison Hight
University of Tennessee - Knoxville, bhight@utk.edu

To the Graduate Council:

I am submitting herewith a thesis written by Brad Harrison Hight entitled "Neutron Imaging of Lithium (Li) Coolants inside High Temperature Niobium (Nb) Heat Pipes." I have examined the final electronic copy of this thesis for form and content and recommend that it be accepted in partial fulfillment of the requirements for the degree of Master of Science, with a major in Mechanical Engineering.

Kenneth D. Kihm, Major Professor

We have read this thesis and recommend its acceptance:

Kivanc Ekici, Rao V. Arimilli

Accepted for the Council:
Carolyn R. Hodges

Vice Provost and Dean of the Graduate School

(Original signatures are on file with official student records.)

Neutron Imaging of Lithium (Li) Coolants inside High Temperature Niobium (Nb) Heat Pipes

A Thesis Presented for the

Master of Science

Degree

The University of Tennessee, Knoxville

Brad Harrison Hight

May 2014

Abstract

Lithium (Li) behavior inside a high temperature Nb-Li leading edge heat pipe was successfully imaged under induction heating operation via neutron imaging. Startup and cool-down operations gave visual confirmation of bulk Li movement using both gravity assisted and inverted operating orientations. The pipe was imaged during an operation cycle from ambient conditions, heated to a steady state temperature of 908.8 ^{0}C, and allowed to cool below 200°C. The experiment was performed at the National Institute of Standards and Technology (NIST) in Gaithersburg, Maryland, and at the Oak Ridge National Laboratory (ORNL) in Oak Ridge, Tennessee.

Tomographic images of the heat pipe sample at ambient conditions were taken at NIST using three 5s exposures combined for each step, with a step angle of 0.18° resulting in 1001 projections. The reconstructed images gave insight into workmanship and Li wetting characteristics of the heat pipe. The cross sectional images allowed for visualization of the sample's inside mesh wicking structure and Li distribution, giving understanding into structural workmanship that is critical for the pipe's working efficiency. The reconstructions were used to create a 3-D rendering of the heat pipe and the inner lying Li distribution.

Comparative heat transfer experiments were conducted for a heat pipe containing non-condensable gases (NCGs) and another sample that was free of NCGs, using a threaded stainless steel water jacket. The heat pipe containing no NCGs resulted in double the cooling heat flux for the same induction heating input power, with a maximum of 440 W being removed from its condenser at an input of 1800 W. The result of the experiment was used in

conjunction with visual observation of the pipes under heating loads to confirm the negative impact of NCGs on a heat pipe.

Future recommendations are to more realistically simulate hypersonic leading edge heating loads using localized heating instead induction heating. A butane-powered portable torch can be considered to localize heating to the leading edge and allow for higher test temperatures. The setup would be done in open air, allowing for combustion but would require a silicide anti-oxidation coating for the tested heat pipe surfaces.

Table of Contents

List of Tables

List of Figures

Chapter 1

Introduction

1.1 Significance

In the business of hypersonic flight, a cooling system is needed for the high temperature leading edges of the vehicle. One proposed solution has been to use liquid metal heat pipes to transfer the heat from leading edges to the cooler interior and therefore reduce centralized heating loads. While the theory of such pipes has been established, more information on actual performance is needed before implementation. Imaging of the liquid working fluid provides a means to characterize each specimen's mass and heat transport and is the focus of this work. Neutron radiography provides an ideal way to non-destructively image such pipes, as it allows for visualization of the inner working fluid while penetrating through the outer hull.

No such imaging tests have previously been conducted on high temperature leading edge heat pipes. With the use of neutron imaging, the pipes are able to be observed while in operation and flow of the working fluid is allowed to be visualized. Heat and mass transfer characteristics are able to be observed along with faults in the pipes' structures which may cause undesirable coolant flow and even structural failure under large heating loads. Previous tests have been used to confirm the feasibility of imaging liquid metal heat pipes [Ref. 7]. Lessons learned have been used to increase the ease of operation and quality of data for the imaged samples.

1.2 Heat Pipes

Heat pipes are passive two phase heat transfer devices that transfer heat through the evaporation of a working fluid (Fig. 1). Capable of providing very high thermal fluxes via latent heat of vaporization, heat pipes can have an effective thermal conductance hundreds of times greater than the best solid metallic conductors. Large amounts of heat can be transferred with a relatively small temperature differential (compared to a solid conductor) and heat pipes generally operate near isothermally once steady state operation has been achieved. A heat pipe consists of an outer envelope, with an evaporator section at one end and a condenser section at the other, which houses a working fluid and capillary wicking structure. It is a closed loop system that transfers heat from one region of the pipe to another by means of a two phase flow cycle [Ref 1].

In operation, heat is applied to the evaporator section and conducted to the working fluid, vaporizing the liquid working fluid. Vaporization increases the vapor pressure in the evaporator, causing vapor, and therefore the latent heat, to flow toward the condenser. Once the vapor reaches the cool condenser, the latent heat is released and the working fluid condenses and is returned to the evaporator by means of capillary action provided by the wicking structure. The capillary forces are automatically developed from the heat transport process.

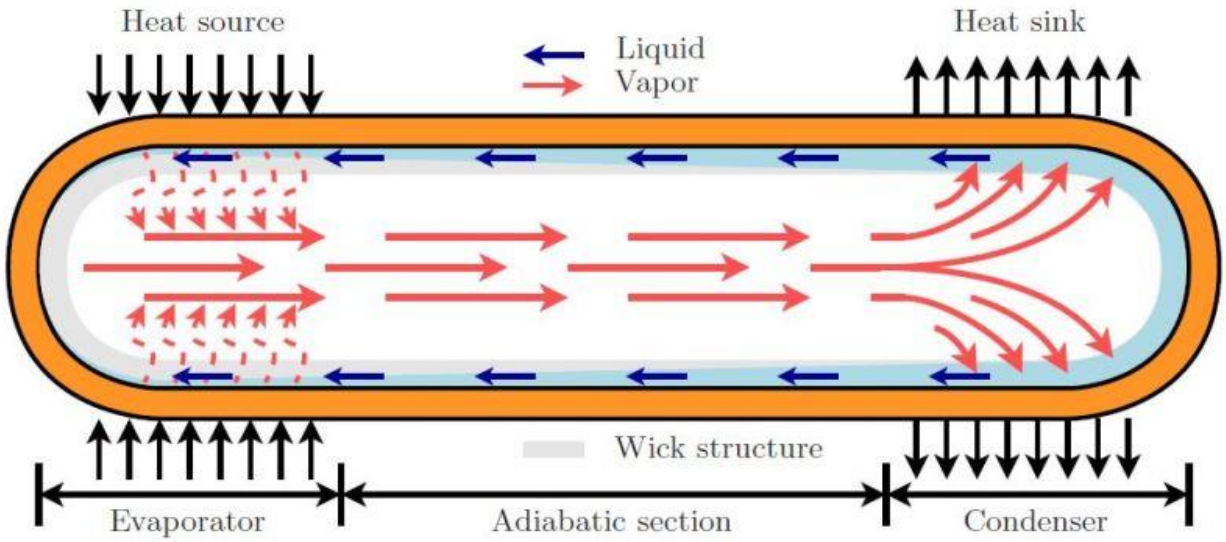

Figure 1 Schematic of Operating Heat Pipe [Ref 2]

Heat pipes have been used and designed for many applications, including electronics, HVAC systems, aerospace, nuclear reactors, cryogenics, and medical equipment to name a few. Although most heat pipes operate in the same way, three main components can vary depending on the specific design criteria required: working fluid, wicking structure, and outer envelope. When selecting a working fluid, the first consideration is the operating temperature. Varying from -271 ^{O}C (Helium) to 2300 ^{O}C (Silver), a wide range of operating temperatures is available (Table 1). Ideally, a fluid needs to have a low viscosity, high surface tension, and be compatible with good wettability on the wick and wall materials for liquid return from the condenser. A compatible vapor pressure is also needed. If the fluid's vapor pressure is too high or too low for the pipe's operating range, the efficiency of the pipe could be limited. [Ref 1]

Table 1 Heat Pipe Working Fluids [Ref 1, 16]

Working Fluid	Melting Point (^{O}C)	Boiling Point (atm. Pressure, ^{O}C)	Useful Range (^{O}C)
Helium	-271	-261	(-271) – (-269)
Nitrogen	-210	-196	(-203) – (-160)
Ammonia	-78	-33	(-60) – 100
Acetone	-95	57	0 – 120
Ethanol	-112	78	0 – 130
Water	0	100	30 – 200
Mercury	-39	361	250 – 650
Potassium	62	774	500 – 1000
Sodium	98	892	600 – 1200
Lithium	179	1340	1000 – 1800
Silver	960	2212	1800 – 2300

The main purpose of the wicking structure is to provide a return passage for the working fluid. For effective transport from the condenser to the evaporator, liquid flow resistance is minimized by large internal pores (or flow channels in the case of axial grooved wicks) that are axial to the flow path. A wick must also have pores at the liquid-vapor interface that are capable of providing the necessary capillary pumping pressure to return the working fluid to the evaporator. Generally smaller surface pores are used for this, as they help generate a large capillary pressure. Finally, the wick must provide a means for heat transfer between the inner walls of the envelope to the working fluid with a minimal temperature differential. Most wicks are made of highly conductive materials (both homogeneous and composite) and can be made in a variety of structures, such as a wrapped screen, annular channel, or axial groove (Fig. 2). [Ref3]

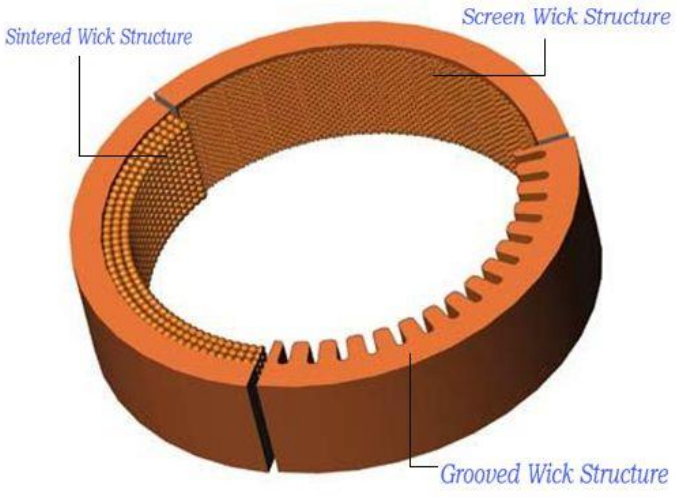

(a) (b)

Figure 2 Common capillary wicking structure types

The outer envelope should be designed with three important ideas in mind: it should isolate the working fluid from the outside environment, be leak proof, and provide a good thermal bridge to the wick structure and working fluid. A material with high thermal conductivity is obviously a necessary choice, but it also needs to be easy to fabricate, weld and have good wettability with the working fluid. Once the pieces of the container are fabricated, they must be cleaned, usually using some solvent or acid treatment, and outgassed. Outgassing of the metal components (including the wick) ensures that no non-condensable gasses (NCGs) will form in the pipe once it has been sealed with the working fluid. If the pipe is not outgassed before it is evacuated, charged and sealed, NCGs could form during the heating process and block off a portion of the condenser, reducing the effectiveness of the heat pipe. [Ref 1]

Heat pipes have several limitations that can impede the pipe's heat flux and depend on the working fluid, pipe geometry, wick structure, and working fluid temperature (Fig. 3). From startup, when the temperature and vapor pressure are low, if the small pressure differential between the evaporator and condenser cannot overcome the viscous friction effects, the vapor flow can be hampered and limit the heat transfer through the pipe (Viscous Limit). Once the working fluid has heated up past the viscous limit (but still with a moderately low vapor pressure) the vapor's velocity at the end of the evaporator can reach the speed of sound and become choked, putting a cap on the vapor flow rate (Sonic Limit). The capillary wicking structure is used to return the working fluid from the condenser to the evaporator. The return of the working fluid is limited by the characteristics of the wick, and if the capillary pressure is too low to overcome the pressure differential in the pipe, dry out can occur (Capillary Limit). As vapor flows from the evaporator to the condenser, it exerts a shear force on the opposing liquid

return in the wick. If the surface tension of the liquid is inadequate, this shear force can entrain small liquid droplets, limiting the return of working fluid and possibly causing dry out of the wick and evaporator (Entrainment Limit). At high operating temperatures, boiling of the working fluid can occur, producing bubbles in the liquid layer. These bubbles can block pores, decreasing liquid and vapor flow rates, and also limit the heat that can be conducted to the working fluid from the outer shell and wicking structure. These effects can limit the pipe's heat flux) and overall performance (Boiling Limit). [Ref 1]

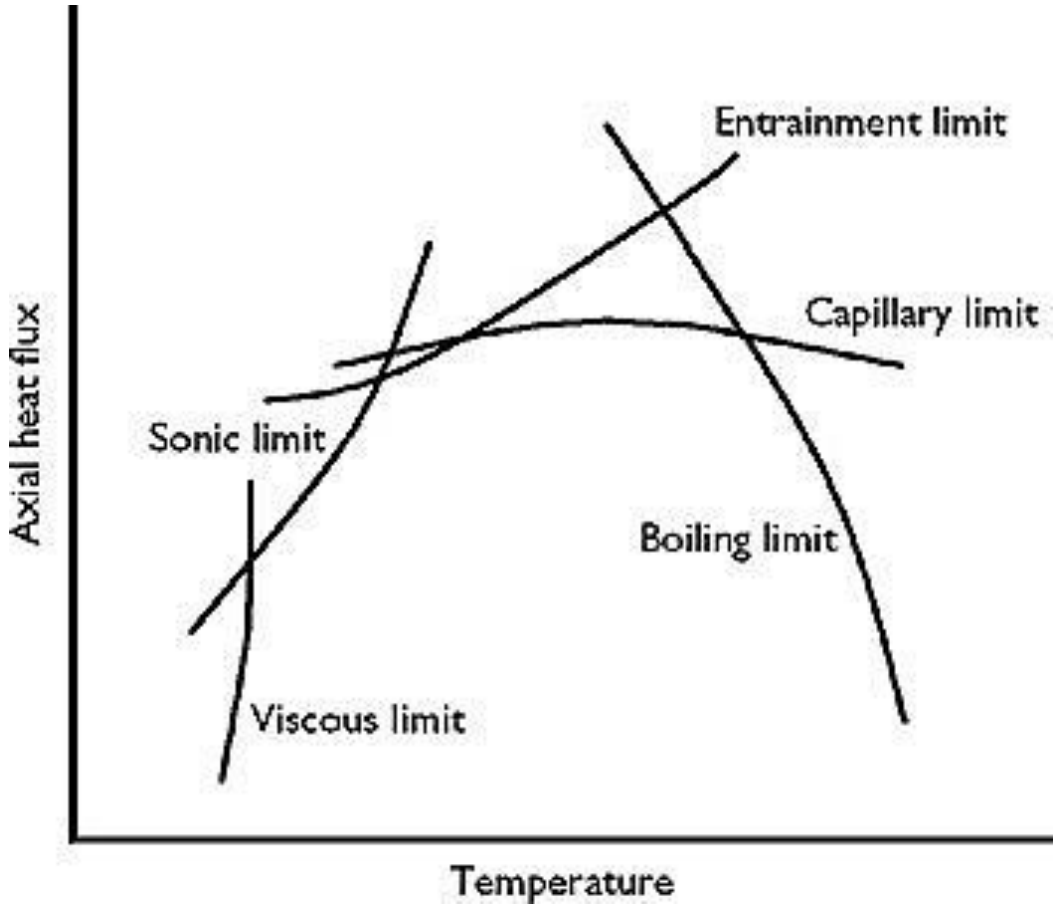

Figure 3 Heat Pipe Operation Limitations [Ref 4]

1.3 Neutron Radiography

Neutron radiography is an efficient, nondestructive tool that can be useful in many research areas and, in particular, imaging. It works similarly to X-ray radiography in that a beam of particles is projected toward a target that absorbs (or scatters) some of these particles and allows others to pass through. A shadow is created that gives a 2-D rendering of the object based on the particles that have penetrated the sample. The intensity of a neutron beam after passing through an object can be predicted using the Lambert-Beer law of attenuation

$$I = I_0 e^{-N\sigma t} \text{ (for an element) or} \quad (1)$$

$$I = I_0 e^{-\sum N_i \sigma_i t_i} \text{ (for a compound)} \quad (2)$$

where I is the intensity after attenuation, I_0 is the incident intensity, N is the atomic number density, σ is the neutron attenuation cross section, and t is the sample thickness [Ref 5, 6, 7].

Neutron radiography differs from its X-ray counterpart in that neutrons interact with an object's nucleus whereas X-rays interact with orbital electrons [Ref 8]. Since neutrons generally do not interact with the orbital electrons, neutron radiography is typically indifferent to an object's density and is more dependent on its chemical composition (Fig. 4). This property is what makes neutron radiography so useful, allowing a heavier, denser element such as Niobium (neutron cross section of 7.3 barns, 1barn=1E-24 cm^2) to be penetrated while some

lighter elements, such as Hydrogen (neutron cross section of 82.3 barns) and Lithium (neutron cross section of 72 barns), can be easily imaged [Ref 9]. Neutron cross sections can also vary between different isotopes of the same element (water and heavy water for instance), which can be useful in many testing areas. While hydrogen in light water (H_20) has a large attenuation cross section (82.36 barn), the deuterium in heavy water (D_20) has a relatively small attenuation cross section (7.64 barn), allowing for objects behind it to be imaged.

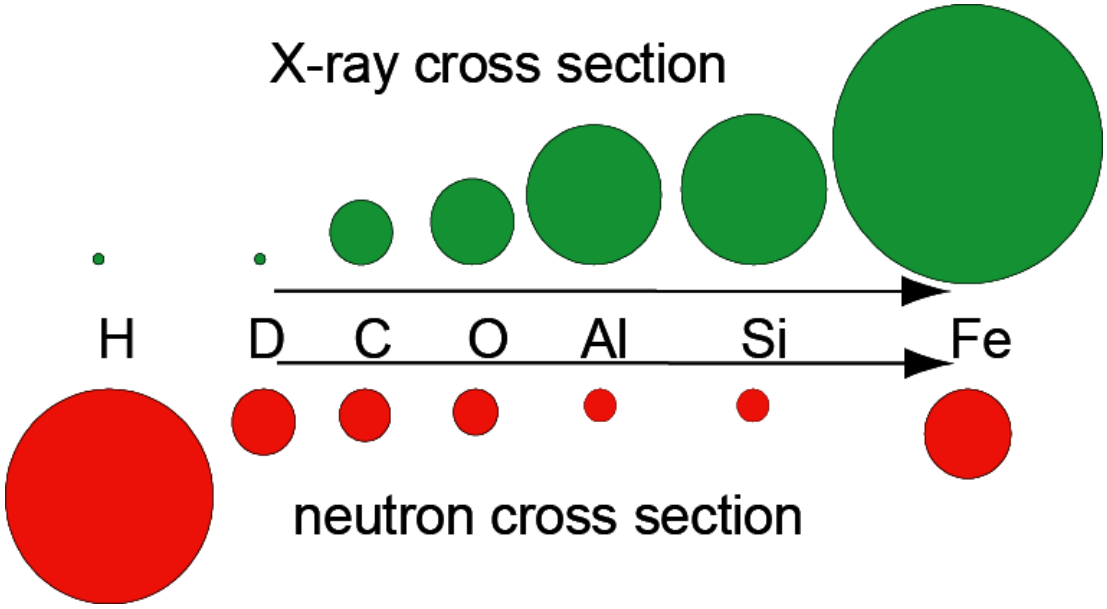

Figure 4 Attenuation characteristics of X-rays compared to those of Neutrons [Ref 12]

The first and obvious requirement for neutron radiography is a source of neutrons. Generally, each source has it's own advantage, such as flux, complexity, and portibilty. There are three general neutron sources: accelerators, radioisotopes, and nuclear reactors. Accelerator neutron sources target an accelerated beam of charged particles at a sample which results in the spalling of neutrons. They have a flux range from 10^7 to 10^{14} n/cm^2/s and range in size and complexity, from smaller portable neutron generator tubes to very large complex spallation facilities.

Radioisotope sources use radioactive isotope decay to generate charged particles (alpha or gamma particles) that bombard a target which in turn emits neutrons, similar to an accelerator source. These sources are generally portable and much more simple than the other source types. They provide lower neutron fluxes, ranging anywhere from 10^5 to 10^9 n/cm^2/s. While they are simple and portable, they do have some major disadvantages, namely the inability to be switched off and a decreasing flux output (as the radioactive isotope decays, its charged particle flux decreases).

The last and most relevant source to this research is a nuclear reactor neutron source. A nuclear reactor uses nuclear fission to produce neutrons and gamma radiation which are then moderated and narrowed into a beam. They provide the most intense neutron beams (along with a few larger spallation sources) with fluxes ranging from 10^{10} to 10^{15} n/cm^2/s or higher. They are, however, generally located in large, complex, and expensive facilities. Since they are so expensive, only a few are availible and acquiring beam time can be difficult. Oak Ridge National Lab's (ORNL) High Flux Isotope Reactor (HFIR) and the National Instute of Standards

and Technology's (NIST) Center for Neutron Research (CNR) are examples of such facilities, which also have dedicated beam lines for neutron imaging.

When a neutron is generated from a source, it contains a very high energy and must be slowed down to be useful for radiography. Sources typically produce fast neutrons (energies anywhere from 0.85 MeV in reactors to 14 MeV in accelerators) which are moderated to the cold-epithermal region (Table 2). The point of the moderator is to remove some of the energy from the neutron (opposed to completely stopping the neutron through absorption), so materials are selected to have low absorption cross sections (maximizes flux) and high scattering cross sections (maximizes energy loss). Common moderators are water, D_2O (heavy water), and beryllium.

Table 2 Neutron Energy Classifications [Ref 9]

Neutrons	**Energy range**	**Wavelength [Å]**	**Velocity [m/s]**
ultra cold	≤ 300 neV	≥ 500	≤ 8
very cold	300 neV - 0.12 meV	52.2 – 26.1	7.5 – 152
cold	0.12 meV - 12 meV	26.1 – 2.6	152 – 1515
thermal	12 meV - 100 meV	2.6 - 0.9	1515 - 4374
epithermal	100 meV - 1eV	0.9 - 0.28	4374 - 13.8 10^3
intermediate	1eV - 0.8MeV		
fast	> 0.8MeV		

During the moderation process, neutrons are randomly scattered and their energies lowered. They must then be shaped into a beam that is useful for radiography, which is done using a collimator. A collimator is a tube that allows neutrons traveling at the desired angle to pass through while blocking all others. They are lined with highly neutron absorbent material, made to prevent low angle scattering and the entering of stray off-angle neutrons. While many collimator designs exist, the most common (and only one used in this research) is a divergent collimator (Fig. 5) which has a small aperture at the entrance that diverges into a larger exit. The angular spread at the end of the collimator depends on its L/D ratio, where L is the length of the collimator and D is the entering aperture's diameter. Changing the L/D ratio changes the beam spread and the neutron flux, with a higher L/D resulting in a greater spatial resolution at the expense of a lower flux. Facilities often have multiple aperture settings to maximize spatial resolution with the highest possible flux [Ref. 11].

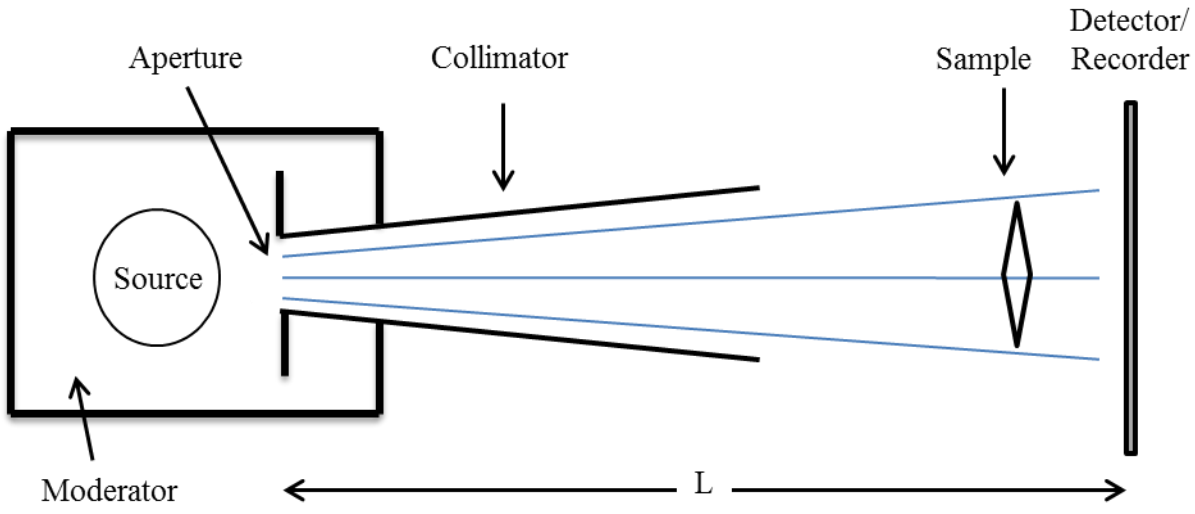

Figure 5 Neutron Imaging Setup

Once a neutron has passed through the sample it reaches a multi-component detector system that is comprised of a converter and a sensor. The converter is a medium which emits some form of radiation, such as an alpha, gamma, or light, when a neutron is absorbed. The sensor detects this radiation and uses it to record the image. For this research, a scintillator screen (a material that absorbs ionizing radiation and emits low energy photons) was used as the converter. Since light is the resulting radiation, they can be coupled with an analog or digital camera image recorder to produce very quick results [Ref 8].

1.4 Oak Ridge National Laboratory (ORNL)

Oak Ridge National Laboratory's (ORNL) CG-1D neutron imaging prototype facility, located in Oak Ridge, Tennessee, is a reactor based neutron source fed from the High Flux Isotope Reactor (HFIR), an 85 MW light water cooled reactor fueled by Uranium-235. CG-1D utilizes helium filled aluminum flight tubes with available L/D ratios ranging from 400-800. The beam can be configured for white beam operation or can operate with a chopper to produce a pulsed beam. Several detectors are available, including a micro-channel plate detector with a 40 micron spatial resolution and LiF/ZnS scintillators varying from 50 to 200 microns. A new imaging instrument, VENUS, is currently under development at ORNL's Spallation Neutron Source (SNS) facility [Ref. 12, 13].

Figure 6 ORNL's CG-1D Neutron Imaging Beam Line

1.5 National Institute of Standards and Technology (NIST)

The National Institute of Standards and Technology (NIST), located in Gaithersburg Maryland, is home to the NIST Center for Neutron Research (NCNR). Its Neutron Imaging Facility (NIF) is located at Beam Tube 2 (BT-2) and provides an intense source of thermal neutrons from its 20 MW heavy water cooled reactor that is filtered with 15 cm of liquid nitrogen cooled bismuth single crystal. L/D ratios ranging from 100 to 6000 are available with a maximum fluence rate of 5.1×10^7 neutrons/cm^2/s for the minimum L/D of 100, along with a 150 micron scintillator. The facility is oriented for both radiographies as well as tomographies, with an emphasis placed on fuel cell research [Ref 14, 15].

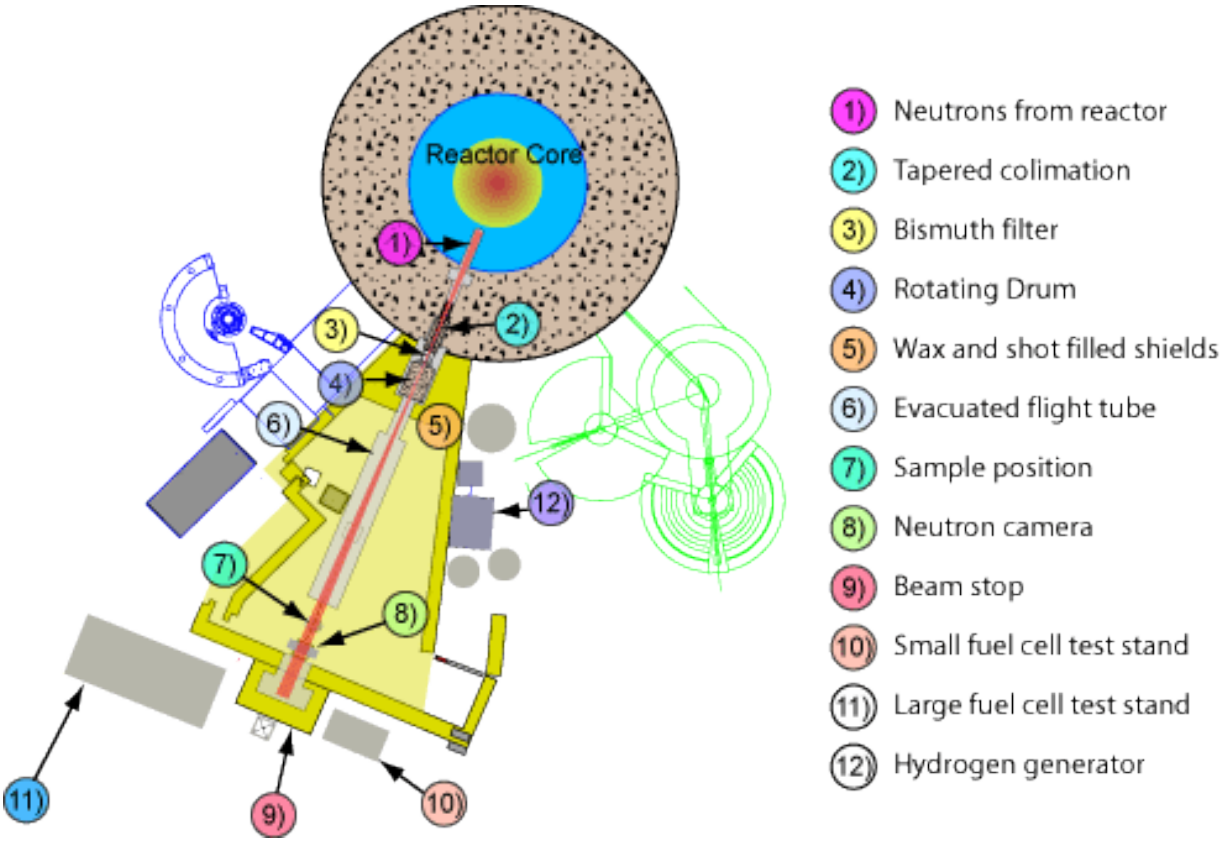

Figure 7 Schematic of NIST's BT-2 Imaging Facility [Ref. 14]

Chapter 2

Test Setup and Procedures

2.1 Leading Edge Nb-Li Heat Pipes

A total of 6 Niobium (Nb) - Lithium (Li) leading edge heat pipes were available for study. Of these, included were an empty shell, two fully operational pipes free of NCGs, and three partially operational pipes containing various amounts of NCGs. The 6” long, ½” by 1” cross sectioned pipes were fabricated with an extruding 1” thick tapered region starting 2 ½” inches from the bottom that made up the leading edge evaporator section, Fig. 8-a. They were constructed with a Nb shell and Molybdenum (Mo) mesh layer wicking structure and each pipe (excluding the empty shell) was charged with 1 g of Li. The Nb shells enabled high temperature functionality while also providing a means to visualize the inner Li working fluid via neutron imaging. Fig. 8-b and 8-c display the difference between a heat pipe with NCGs (Fig. 8-b) to that of one free of NCGs (Fig. 8-c) during operation. It should be noted that almost all of the condenser for Fig. 8-b has been completely blocked off by NCGs while the condenser for Fig. 8-c is fully operational.

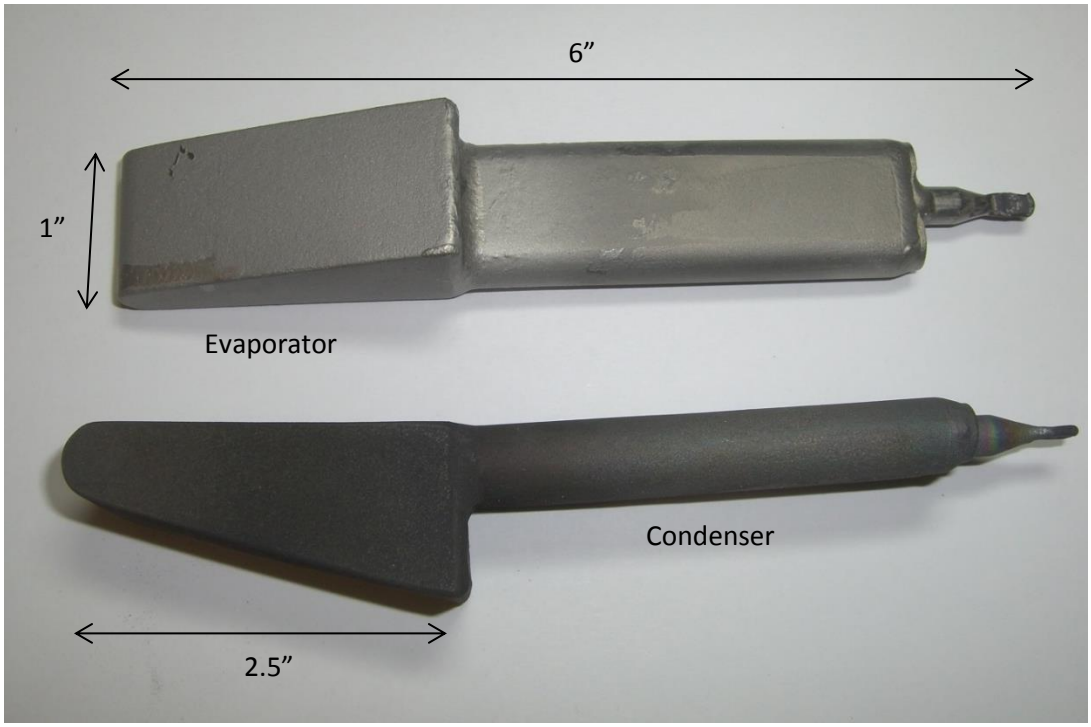

(a)

(b)

(c)

Figure 8 Nb-Li Leading Edge Heat Pipe Samples. Note: the bottom sample in (a) is protected with a silicide coating to prevent oxidation and is why it appears “charred”

2.2 Testing Setup

To keep the heat pipe samples from oxidizing at high temperatures, a vacuum testing apparatus was required (Fig. 9). Sample testing was conducted in a vacuum sealed 11.8" diameter stainless steel service well designed with four adjacent ports, two 2.75" CF flanges and two KF40 ports, used for an RF electrical feed through, a K type thermocouple feed through, and a turbo vacuum pump. A ¼" thick, 12" inner diameter fused quartz bell jar with a Viton seal was placed on the top rim on the service well, allowing for both optical and neutron visualization of the interior setup. Heat pipe samples were suspended above the lip of the service well by an aluminum stand and were held using an optical clamp and a thermally insulative ceramic material to minimize conductive losses through the stand. The stand could be easily maneuvered, allowing for heating simulations for gravity assisted (evaporator at the bottom), gravity resisting (evaporator at the top), and horizontal heat pipe orientations.

Close fitting copper induction coils attached via the RF feed through port were used to achieve heating loads and were powered using a 2.4 kW Ambrell EasyHeat RF induction heating system. The coils and EasyHeat induction system were cooled using a FlowMax water circulator, preventing excess heating of the system's electrical components. Four K type thermocouples were connected via the feed through and used to monitor the samples' evaporator and condenser region temperatures as well as the temperatures of the aluminum stand and the bell jar's Viton seal to ensure they stayed below a reasonable value. Temperature data were transferred and recorded through a data acquisition system (DAQ) attached to a laptop computer. During prolonged heating periods, aluminum and molybdenum foil were used as

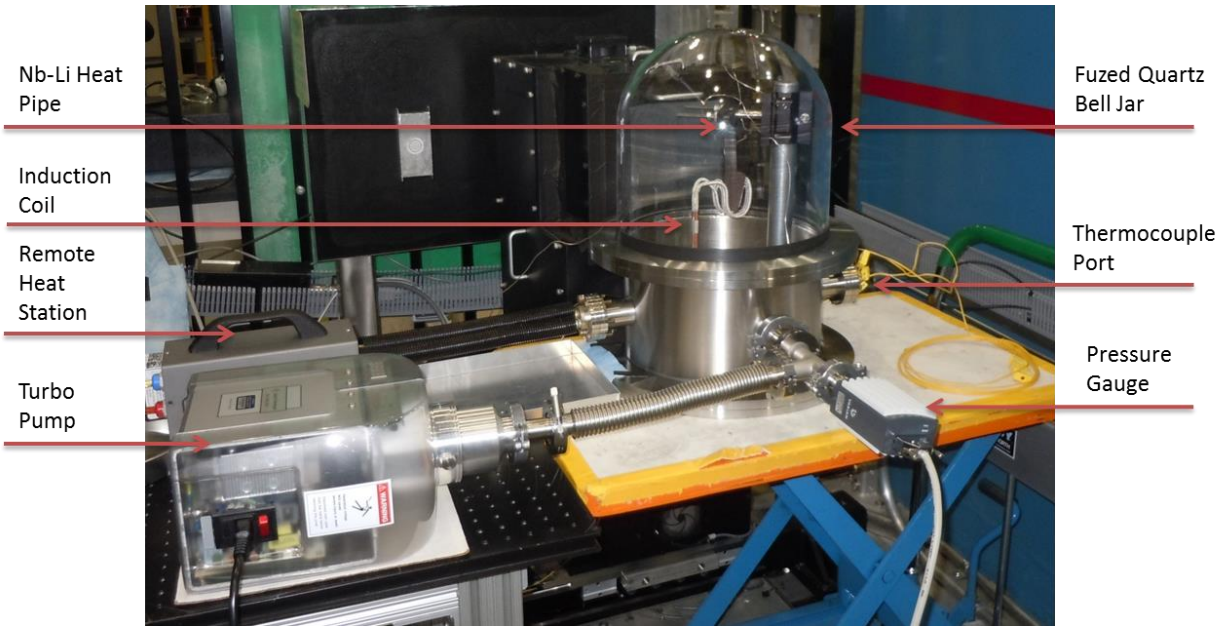

Figure 9 Experiment Radiography Setup on the CG-1D Beamline

radiation shielding to guard the plastic thermocouple connectors and holding stand. Vacuum within the testing apparatus was achieved using an Agilent Technologies turbo pump attached to one of the service well's port flanges. The pressure was monitored from a digital display attached to a cold-cathode ion pressure gauge capable of reading pressures ranging from atmospheric conditions (~750 Torr) down to 3.8×10^{-10} Torr.

The heat pipes were also tested using an experimental heat transfer setup, Fig. 10. The setup was designed to obtain cooling heat flux measurements for a pipe under operation and to compare the cooling efficiencies of a heat pipe with no NCGs to that of one containing NCGs. It used a water jacket consisting of copper coiling coils wrapped around a grooved stainless steel insert that housed the condenser region of a leading edge heat pipe. In order to minimize

radiation heat flux from the evaporator surface, the cooling coil was wrapped with aluminum foil, which acted as a radiation shield (Fig. 10-c). Two thermocouple probes placed at the inlet and outlet of the cooling coils were used to monitor and record the difference between the inlet and outlet coolant temperatures. Two more thermocouples were placed on the inserted heat pipe's evaporator and condenser regions. The experiment was conducted in the same vacuumed apparatus as previously mentioned, with the addition of the water jacket and the heat pipe holding stand removed. An additional RF feed through was used in this experiment to connect the cooling coils of the water jacket to a variable temperature water chiller. The mass flow rate of the coolant was controlled and recorded using an Omega rotameter with a precision of 0.05 liter per minute (LPM).

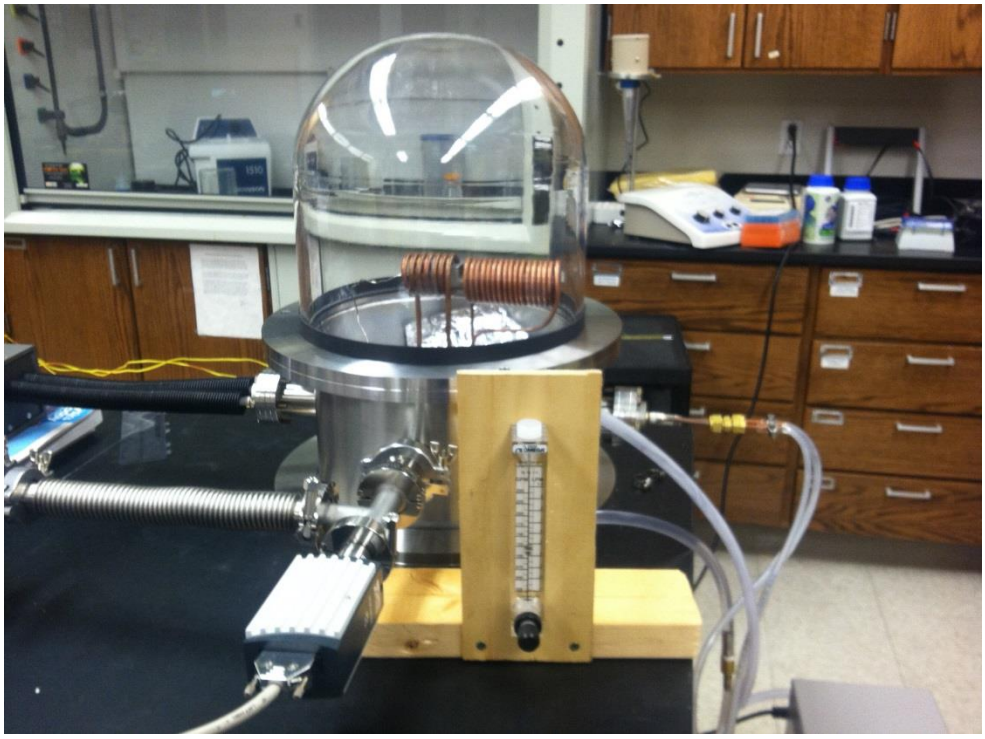

(a) Overall experimental layout to measure the cooling heat flux amounts for the Nb-Li heat pipe inside a vacuum bell jar.

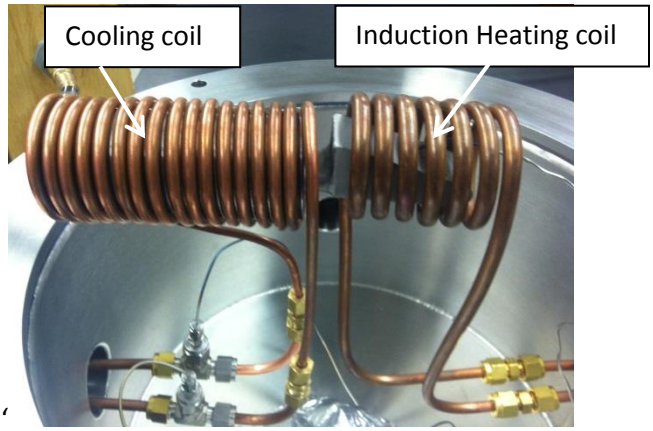

(b) Unshielded cooling coil

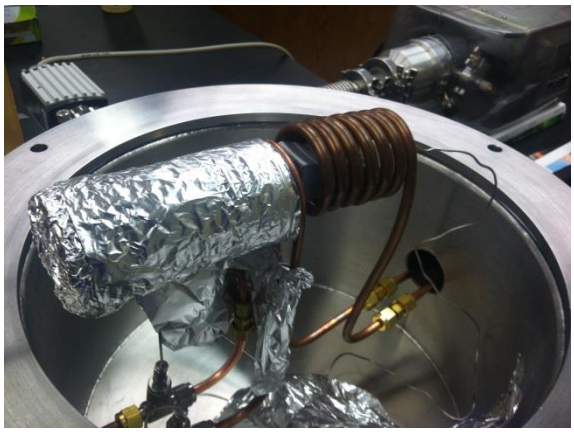

(c) Radiation-shielded cooling coil

Figure 10 Experimental setup to measure the cooling heat flux vs. the heating power input.

2.3 Experiment Procedure

To begin the imaging experiment, the test platform was assembled with the desired heat pipe orientation and the system pumped to a pressure below $5x10^{-4}$ Torr, allowing for safe operation of the heat pipes without oxidation of their Niobium shells at high temperatures. All electrical lines, namely those connecting the remote heat station to the electrical flanges, required protective coverings to prevent anything touching the exposed power lines. Protective absorbent material was placed under the water lines connecting the induction power supply to the service well in case of any leaks or spills of fluids that had seen the beam. When at NIST, D_2O was provided and used as a coolant for the induction system instead of H_2O. D_2O, while expensive, has very similar physical and thermal properties as light water but with the added benefit of being transparent to neutrons, allowing for visualization through the copper induction coils.

Once an adequate pressure was achieved and the system was checked for leaks, a preliminary bake out test to 500°C was performed to burn off any oils, greases, or residues that were on the inside of the testing apparatus. The burning of unwanted surface contaminants increased the overall pressure inside the vessel which would then be allowed to pump back down an accepted value. Preliminary heating ensured that the pressure would remain as steady as possible during an actual imaging test.

With the apparatus on the imaging stand and the bake out complete, the desired sample region would be positioned using cold images. This consisted of short exposure times, just enough to check the position of the heat pipe, with the stand and shutters being adjusted

appropriately. Starting from ambient conditions, the sample would be imaged and heated to a desired steady state temperature, with a maximum of 1150^{o}C, and held at that temperature for a designated amount of time. Imaging would proceed through the steady state period and continue while the sample cooled to a temperature below 200^{o}C, effectively giving visualization of a pipe's complete working cycle. Temperature data were recorded and closely monitored during the heating process, along with the internal pressure of the system. If any temperature reading exceeded 1150^{o}C or the pressure rose above 9x10^{-4} Torr, power to the system would immediately be shutoff, the pipe allowed to cool to below 200^{o}C, and the pressure allowed to lower before running another test. Sample exposure times ranged from 5 minutes to 1 hour with 0.5s to 4s per image and pixel binning from 1x1 to 4x4. Longer exposures give better spatial resolution at the cost of missing dynamics, so often multiple tests were done for the same setup to get the optimum combination of exposure time with binning.

Tomographic imaging was done for each cold heat pipe sample. The pipes were held in an aluminum tube, rotated 180^{0}, and imaged at small rotation angles to get a full 3-D rendering. Depending on the amount of time given for each tomography, the exposure time and rotation angle could be adjusted to get maximum spacial resolution with maximum amount of exposure. For heat pipe #1, a rotation step of 0.18^{0} was used from 0^{0} - 183^{0} (to make sure all 180^{0} were accounted for) to give a total of 1001 projections with three 5s exposures combined at each step. Image normalizations for the heating tests were conducted at UT using iMars software provided by ORNL. Tomographic reconstructions were done at ORNL using Octopus software.

The same pressure and preliminary bake out procedures for the heated imaging tests were required for the cooling heat flux experiments. For these experiments, a prolonged heating period was planned, requiring a lower starting vessel pressure. The system was left over night to pump down to below $5x10^{-5}$ Torr, or lower if possible, to compensate. For each test, power inputs starting from 800 W and going to 1800 W with a step increase of 100 W were applied to the heat pipe sample. The pipe's evaporator and condenser regions, as well as the inlet and outlet temperatures of the water jacket, were allowed to reach steady state temperature at each input and the steady state data were recorded. After about 15s of data recording, the input power was increased by 100 W and the procedure was repeated for the next input. This was done a total of four times using heat pipes #1 and #4, with a total of two complete tests for each pipe (done for repeatability).

Chapter 3

Results and Discussion

3.1 Leading Edge Heat Pipe Radiography

Heat pipe #1 (HP1) was successfully imaged while under heating operation at NIST's BT-2 beam line. Beginning from a cold state, multiple orientations were imaged and are presented in Fig. 11 (gravity assisted) and 12 (inverted). The pipe was heated from ambient temperature to a maximum of 908.8^{o}C and allowed to cool again with a total run time of 10 minutes (from cold to maximum input back to cold). Startup mechanics were observed for both orientations. Fig. 11-a is a radiograph of the pipe at a cold state in a gravity assisted position, Fig. 11-b is at a temperature around 300^{o}C (1:45 after startup), and Fig. 11-c is at a temperature around 250^{o}C during cooling (9:45 after startup). Throughout the pipe's heating cycle, visual displacement of the Li working fluid was evident. If the pictures are analyzed closely, changes can be seen (the movements are more prevalent when all the images are compiled into a movie which is unable to be presented in this paper). To increase visualization, a difference between images was taken to show the changes from the previous state. Fig. 11-d and 11-e are the image differences, with the brighter white sections displaying the change from the first image to the second. Fig. 11-d is a difference between Fig. 11-a and 11-b (d = b - a) and Fig 11-e is a difference between Fig. 11-b and 11-c (e = c - b). A bulk of lithium may be seen rising in the middle of the condenser which can be clearly visualized by Fig. 11-d (blue line). This bulk was not present at startup, but rose into the condenser region once a heating load was applied.

Once the heating cycle had been completed and the pipe had cooled, the Li was pulled back into the evaporator due to capillary forces and the centralized Li bulk could no longer be found (Fig. 11-e). A small chunk of Li (red line) trapped in the mesh structure (present in Fig. 11-a and 11-b) was also found to have disappeared once the pipe had cooled. This was more than likely due to the capillary forces caused by the high surface tension of Li which increases with decreasing temperature.

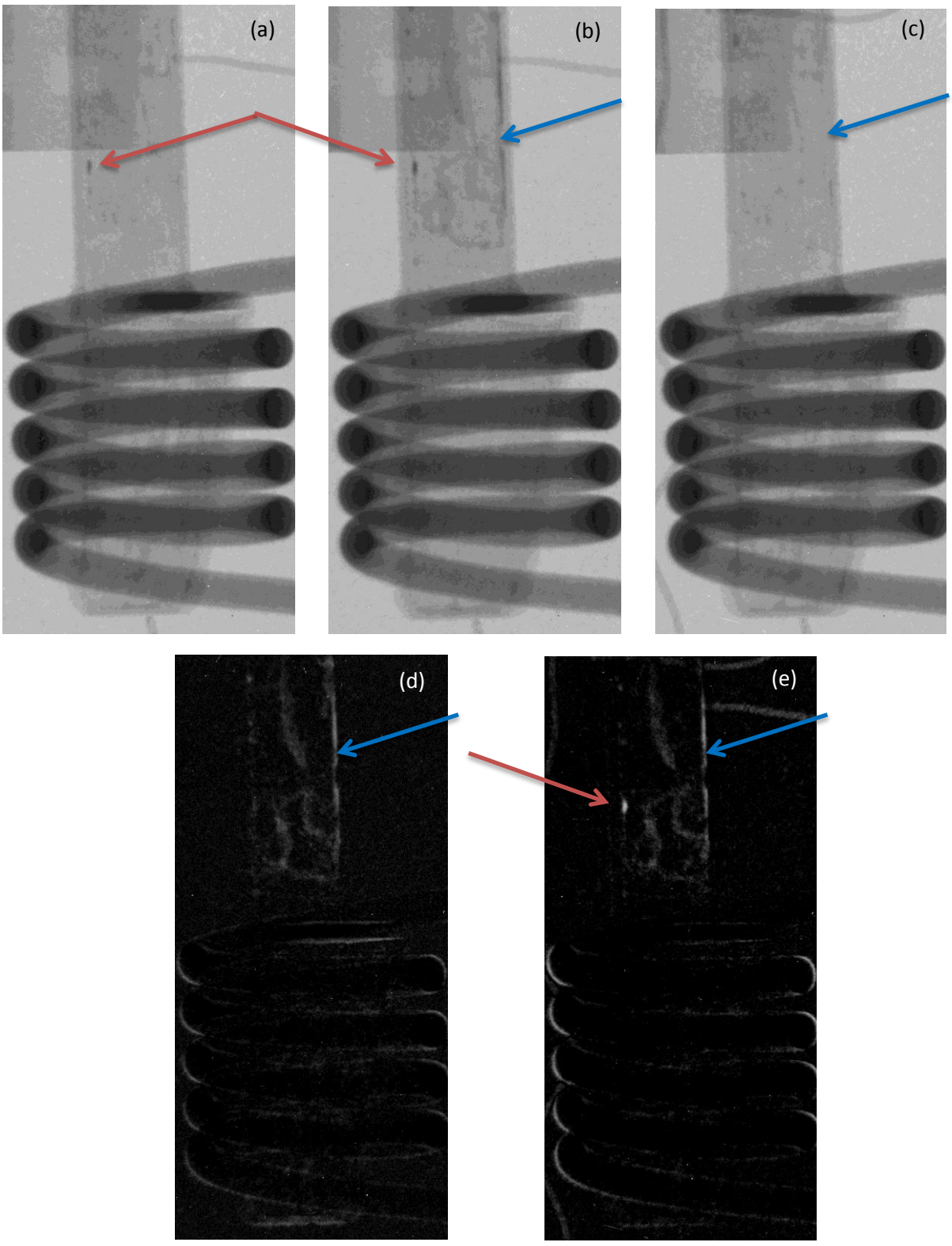

Figure 11 Dynamic imaging of HP1 in a gravity assisted orientation: (a) startup, (b) maximum input, (c) cool down, (d) difference of a and b, (e) difference of b and c

HP1 demonstrated similar startup mechanics in the inverted orientation. Fig. 12-a displays a radiograph at ambient conditions, Fig. 12-b is at a temperature around 450 ^{0}C (0:30 after startup), and Fig. 12-c is at a temperature around 275^{o}C during cooling (6:30 after startup). Although large movements are more difficult to see in the radiographs for this orientation, a difference between Fig. 12-a and 12-b (shown as Fig. 12-d, d = b - a) shows clear signs of Li movement. In particular, the walls of the evaporator section were shown to hold less Li as the pipe was heated up. During cooling, the surface tension of the liquid Li caused it to return to the evaporator walls where it solidified, as can be seen by a difference between Fig. 12-b and 12-c (presented as Fig. 12-e, e = c - b). These may be seen by the blue lines. It may be noted that there is a bright white section on the outside of the pipe's evaporator along with several of the induction coils; this may be attributed to shifting in the pipe and coils due to heating and is not attributed to Li movement.

During steady operations at high temperatures (after startup and before cool-down), not much Li movement was seen. The radiograph movies displayed a quite operation, with little or no evident differences at steady state. Once the pipe is in steady operation, the Li should be moving in a liquid-vapor cycle with liquid return only on the walls drawn by the high capillary forces of the mesh and the high surface tension of the Li. From our radiographies, large Li bulk movements were seen primarily during startup and cool-down when relatively large amounts of liquid Li were moving and condensing. Vapor visualization has been unsuccessful and may be cause for future study along with closer observation of dynamic movement at high operating temperatures.

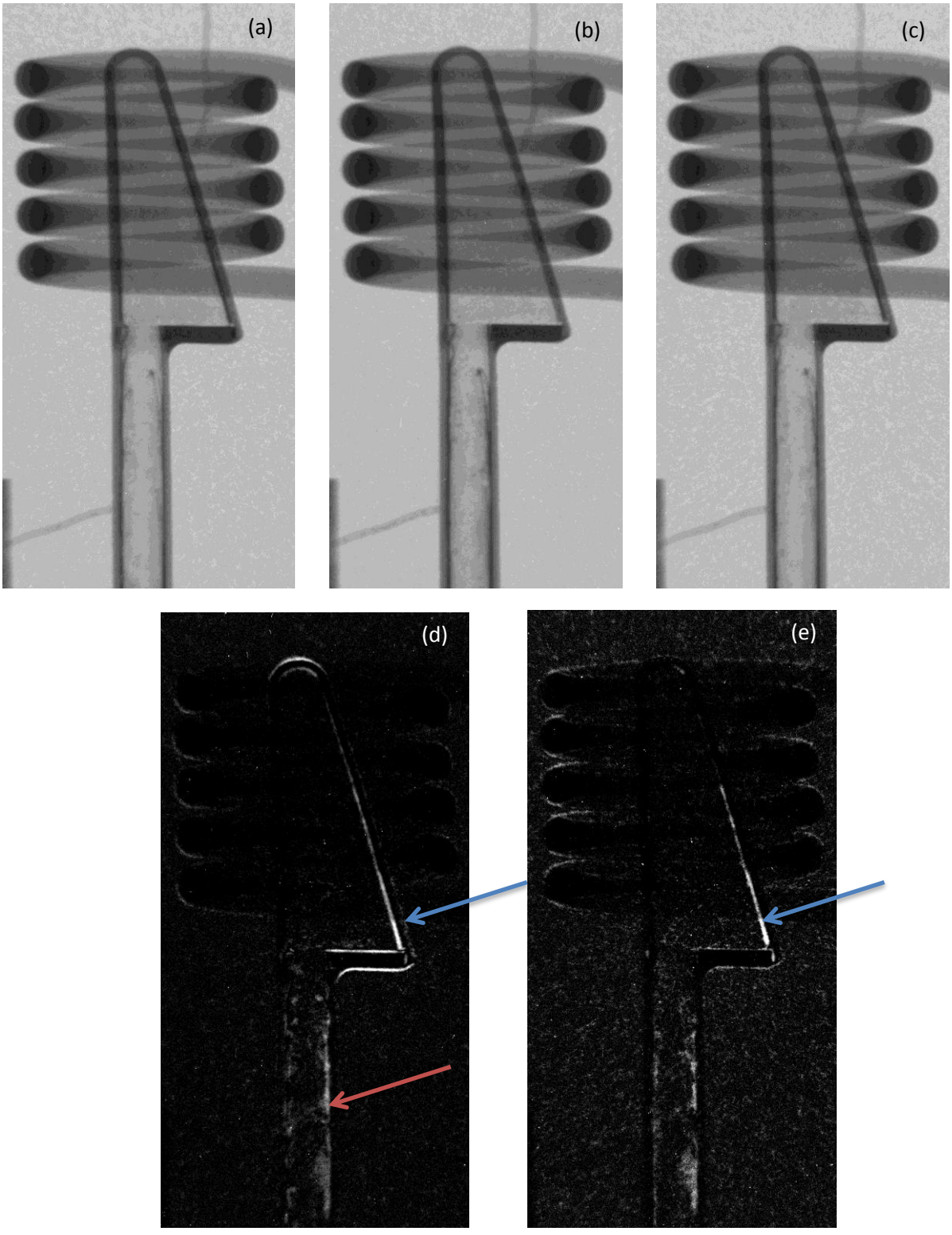

Figure 12 Dynamic imaging of HP1 in a gravity resisting orientation: (a) startup, (b) maximum input, (c) cool down, (d) difference of a and b, (e) difference of b and c

3.2 Leading Edge Heat Pipe Tomography

Computed tomographic (CT) imaging of HP1, free of NCGs, was successfully completed at NIST and reconstructed at ORNL using Octopus software. While such imaging does not give detailed operational information, CTs can give great insight into the workmanship and wetting characteristics of the Li working fluid. Once reconstructed, a CT image sequence presents the sample by its cross sectional slices from top to bottom. For a heat pipe, these slices show the physical layout of the mesh layer and Li distribution at that particular slice. Fig. 13 displays three different sections of HP1 (distances marked from the bottom of the evaporator): a portion of the evaporator leading to the top of the wedge (Fig. 13-a) 1.8" from the base, a section at the top of the wedge (Fig. 13-b) 2.9" from the evaporator base, and a slice in the pipe's condenser (Fig. 13-c) 5" from the base. In these images, the pipe's outer shell, inner mesh wicking structure, and Li distribution within the wick are clearly visible. In design, the wick is supposed to lay flush against the outer Nb shell. These images provide evidence of structure detachment in several portions of the pipe which could cause poor Li return in/through those areas. Li deposites may be seen as brighter lines in the mesh structure, with some areas, the detached mesh portions in particular, void of Li. It may be noted that at the top of the wedge, the mesh layer seems notcibly wrinkled. The two pieces, the wedge evaporator and the oval condenser, were welded at this joint and seems to cause a common mesh laying flaw in the leading edge heat pipes. Large faults like these can cause choke points that severely limit the return of Li to the evaporator.

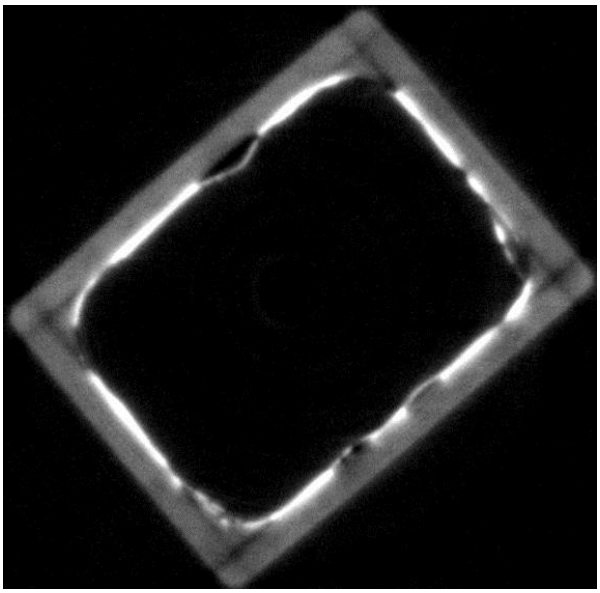

(a)

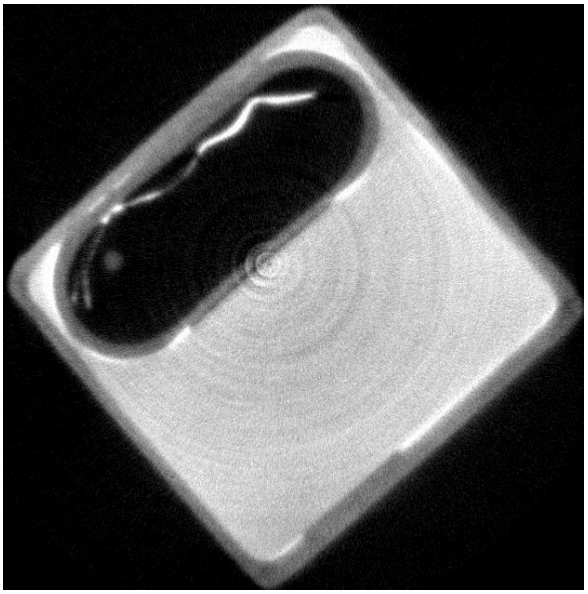

(b)

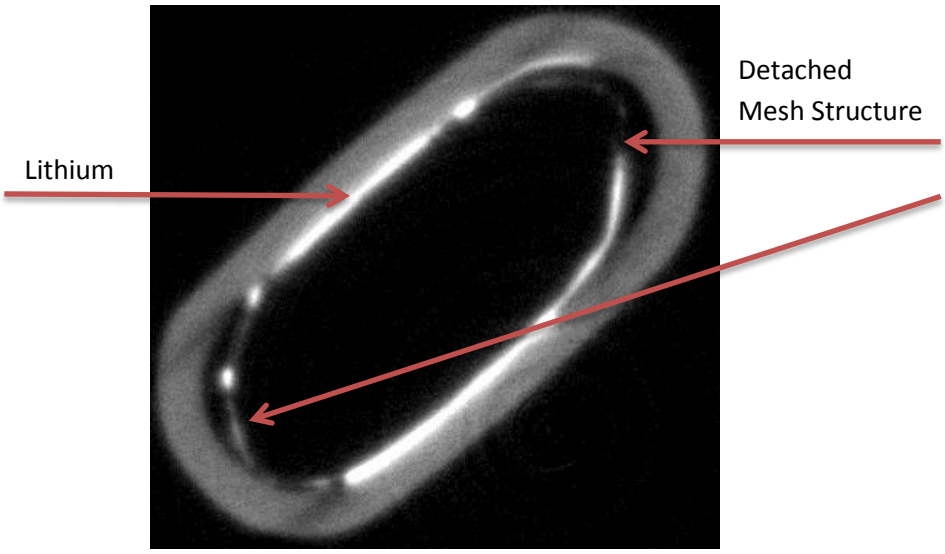

(c)

Figure 13 Reconstructed slices of a computed tomography of Heat Pipe #1: Evaporator (a), Top of Evaporator, (b), and Condenser (c). Li deposits are recognized as the lighter segments in the mesh layer.

Using Image J's volume viewer plugin, the CT reconstructions were used to create a 3-D rendering of HP1, Fig. 14. The images give an overall look at the pipe and give useful visualization of the inside Li layout. The colors represent an arbitrary intensity scale caused by a difference in neutron attenuation throughout the sample. As the threshold is increased, larger intensity (higher attenuation) is shown deeper into the sample. The inner shell (pink color seen at the top of the condenser) is shown to be more intense than the outer, and the lithium layer is a bright yellow (Fig. 14-b) in comparison to the shell's purple hue (Fig. 14-a). Large gaps at the bottom of the pipe and at the evaporator-condenser weld joint are noticeably visible. [Ref 17, 18]

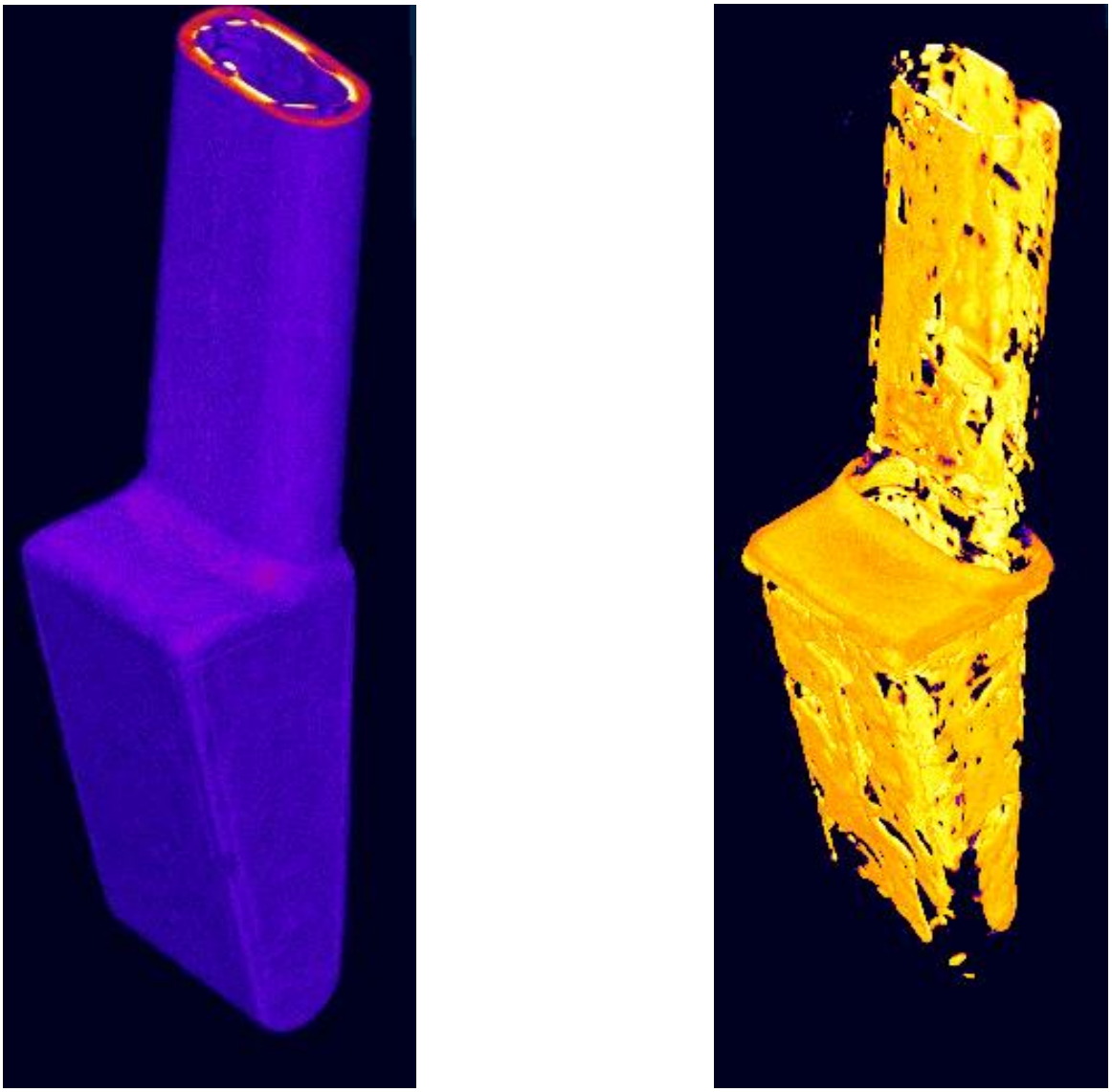

(a) (b)

Figure 14 3-D volumes made from reconstructed slices from a CT of Heat Pipe #1: Nb Shell (a) and Underlying Lithium Distribution (b).

3.3 Cooling Heat Flux Experiment

The purpose of the cooling heat flux experiment was to determine and compare the cooling effectiveness of two separate heat pipes, one containing NCGs and the other being free of NCGs. Heat removed through the coolant water flow at the condenser was determined from the calorimetric energy balance equation, i.e., $q_{out} = \left(\dot{m} c_p \Delta T\right)_{coolant}$, where $\dot{m}$ was the coolant mass flow rate in kg/s, c_p was the specific heat of the coolant water in kJ/kg·K, and ΔT was the temperature differential between the coolant inlet and outlet in K. A differential between the heater power input (q_{in}) and the cooling heat output (q_{out}) was found and can to be primarily attributed to the cooling efficiency of the heat pipe, in addition to energy lost during induction heating and conduction/radiation losses to the environment. Due to its close proximity to the power lines, the RF electrical feed through port on the service well became very hot (over 100 ^{0}C) when power was applied. This noticeable energy loss associated to joule heating of the service well was unavoidable and was a large source of the inconsistency.

The results of the cooling heat flux experiment are displayed by Fig. 15. Two Nb-Li heat pipe articles were tested: heat pipe # 3 (HP3) and heat pipe #4 (HP4). HP3 was free from NCGs and HP4 contained some amount of NCGs, effectively blocking part of its condenser section. HP3 showed better performance under the same q_{in} than HP4, with over double the output (q_{out}) (Fig. 15-a). At a maximum power input of 1800 W, HP3 displayed an output of 420 W compared to HP4 with an output of 207 W. It was apparent that the NCGs of HP4 reduced the effective condenser region and subsequently lowered the heat pipe efficiency. The lowered cooling efficiency of HP4 resulted in the higher evaporator temperatures ($T_{Evaporator}$), in

comparison to HP3, with its evaporator region staying a consistent 75 ^{0}C higher than that of HP3 (Fig. 15-b). At maximum input, HP3 was heated to a maximum of 958 ^{0}C while HP4 was recorded at 1015 ^{0}C. The coolant inlet temperature was kept constant at 18°C and the coolant flow rate was also kept constant at 0.5 L/min for all of the tested conditions.

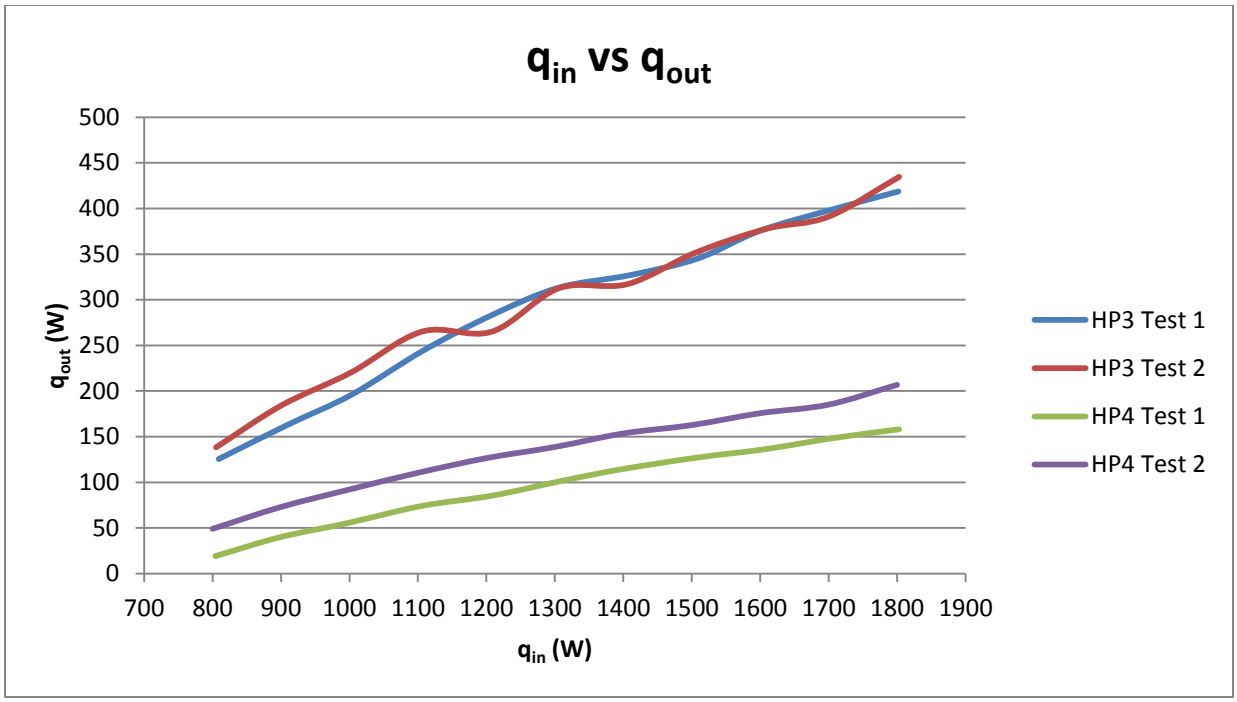

(a)

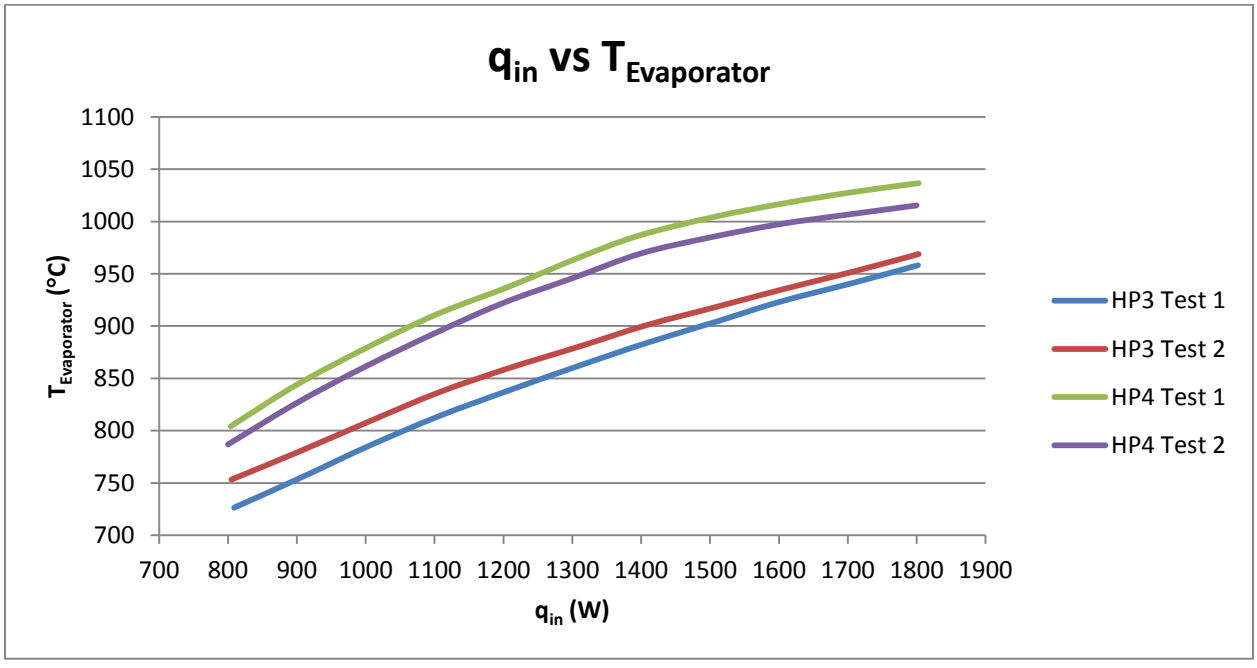

(b)

Figure 15 Heat pipe operational thermal data for the two Nb-Li heat pipe articles, HP3 (no NCG inside) and HP4 (containing NCG): (a) the cooling heat output vs. the heater power input, and (b) the evaporator temperature vs. the heater power input.

3.4 Recommendations

Future testing will focus on higher heat loads concentrated on the leading edge of the evaporator's tip. These will be used to achieve the optimal temperature range for a Li heat pipe, 1000 – 1800 ^{0}C, which would be present during hypersonic flight. The proposed setup is to use a butane-powered portable torch to create a more localized heating to the leading edge and allow higher test temperatures (Fig. 16-a). A flame deflector would help to confine the torch flame to be localized for the leading edge. Since the proposed study with a torch flame should be conducted in open air, the Nb shell of the heat pipe prototype would have to be coated for anti-oxidation with silicide compound (Fig. 16-b). The platform for such a test is still under development and is the main task ahead in regards to the leading edge samples.

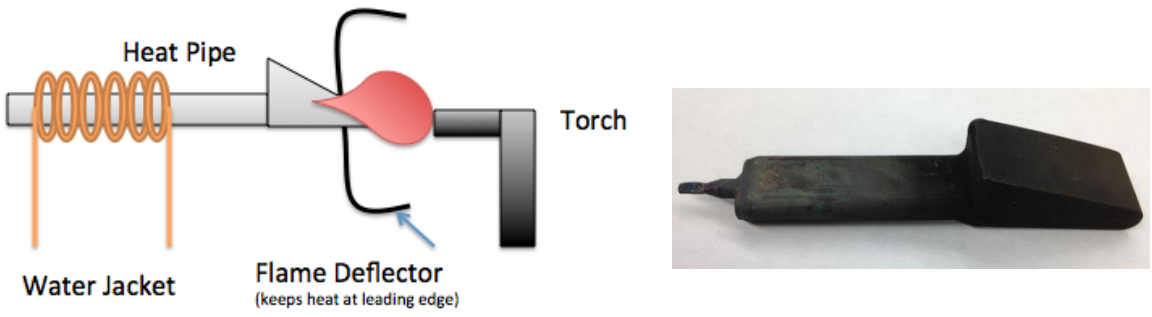

(a) (b)

Figure 16 (a) Schematic of the butane torch heating experimental setup and (b) the Nb/Li heat pipe coated with silicide for anti-oxidation

Chapter 4

Conclusions

Nb-Li leading edge heat pipes under high temperature operating conditions were successfully imaged for the first time utilizing neutron beam lines. Using multiple orientations, bulk Li movement was observed during the startup and cool-down of a functional heat pipe free of NCGs. Although quiet operation was observed for the high temperature steady state operating condition, neutron imaging was confirmed to capture Li flow patterns within the pipe. While this setup worked well for imaging and confirmed Li movement, it did not accurately simulate heating loads of a hypersonic vehicle's leading edges. These loads should be concentrated at the tip of heat pipe's evaporator, a result difficult to emulate using induction heating, and should provide a higher operating range of 1200-1400°C.

Tomographic images of a heat pipe sample at ambient conditions were successfully recorded and reconstructed. The reconstructions allowed for detailed analysis of the sample's workmanship and Li wetting characteristics, giving clear distinctions between the pipe's outer hull, mesh wicking structure, and Li distribution. Flaws in the mesh structure were found, particularly at the weld joint of the evaporator and condenser, which could have been the cause of poor Li return within the sample. The reconstructions were used to create a 3-D rendering of the heat pipe that allowed for a holistic view of the Li working fluid distribution.

A heat transfer experiment was conducted using two separate heat pipe samples, one containing NCGs (HP4) and the other free of NCGs (HP3), using a stainless steel water jacket

wrapped by copper cooling coils. It was shown that HP3 had over double the cooling heat flux of HP4, with a maximum of 440 W being removed from its condenser with an input of 1800 W. Although this seemed like a large discrepancy for power input vs. heat output, the experiment layout was prone to large energy losses due to the induction lines running very close to the large stainless steel service well used to house the test. This experiment, along with visual observation from the two operating pipes, helped confirm the detrimental impact of NCGs on a heat pipe's performance capabilities.

A new experimental setup is under development that should allow for a more accurate simulation of hypersonic flight conditions. The proposed setup utilizes a butane-powered portable torch to create localized heating load at the leading edge and allows for higher operational temperatures. It would be an open air test, due to the combustible gases, and would require a silicide coating on the heat pipe samples to prevent oxidation at high temperatures.

References

1. Zohuri, B., Heat pipe design and technology: a practical approach. 2011: CRC Press.
2. "Heat Pipe .nl." *Heat Pipe .nl*. N.p., n.d. Web. 28 Jan. 2014.
3. Chi, S., Heat pipe theory and practice: a sourcebook. 1976. pp. 3-11.
4. Kew, P.A. " 2.2: OPERATION OF HEAT PIPES." *On GlobalSpec*. N.p., n.d. Web. 28 Jan. 2014.
5. C. Wilson, B. Borgmeyer, R. A. Winholtz, H. B. Ma, D. L. Jacobson, D. S. Hussey, and M. Arif. "Visual Observation of Oscillating Heat Pipes Using Neutron Radiography", Journal of Thermophysics and Heat Transfer, Vol. 22, No. 3 (2008), pp. 366-372.
6. Sears, Varley F. "Neutron scattering lengths and cross sections." *Neutron news* 3.3 (1992): 26-37.
7. Kihm, K., E. Kirchoff, M. Golden, J. Rosenfeld, S. Rawal, D. Pratt, A. Swanson, H. Bilheux, L. Walker and S. Voisin (2013). "Neutron imaging of alkali metal heat pipes." Physics Procedia 43, pp. 323-330.
8. Anderson, Ian S., Robert L. McGreevy, and Hassina Z. Bilheux. "Neutron imaging and applications." *Springer Science+ Business Media* 200.2209 (2009): 987-0. pp. 67-80
9. Lehmann, Eberhard. "What is Neutron Imaging ?" Paul Scherrer Institut (PSI) ::. 24 Feb. 2014 <http://www.psi.ch/niag/what-is-neutron-imaging>.
10. Munter, Alan. "Neutron scattering lengths and cross sections." Neutron scattering lengths and cross sections. 07 Jan. 2013. 25 Feb. 2014 <http://www.ncnr.nist.gov/resources/n-lengths/>.
11. Sharpe, R. S. Research techniques in nondestructive testing. London: Academic P, 1970.

12. "Reactor Technical Parameters." HFIR Technical Parameters. 21 Mar. 2014 <http://neutrons.ornl.gov/facilities/HFIR/techparameters.shtml>.
13. "Instrument Fact Sheet: CG-1D Beamline: High Flux Isotope Reactor: Neutron Imaging Prototype Facility." Oct. 2013 (Mar. 2014)
14. Jacobson, David. "NIST: NIF - Neutron Imaging Facility." NIST: NIF - Neutron Imaging Facility. May 2006. (March 2014) <http://physics.nist.gov/MajResFac/NIF/facility.html>.
15. Jacobson, D., M. Arif, P. Huffman, and R. Satija. "A New Neutron Imaging Facility at BT-6 for the Non-Destructive Analysis of Working Fuel Cells." A New Neutron Imaging Facility at BT-6 for the Non-Destructive Analysis of Working Fuel Cells. 21 Mar. 2014 <http://www.ncnr.nist.gov/AnnualReport/FY2003_html/RH2/>.
16. P. Dunn and D. Reay, *Heat Pipes, 4th ed.*, (Elsevier Science Ltd, New York, 1994), pp. 108, 318-326).
17. K. D. Kihm, B. Hight, E. Kirchoff, H. Yi, J. Rosenfeld, S. Rawal, D. Hussey, D. Jacobson, H. Bilheux, L. Walker, S. Voisin, D. Pratt, and A. Swanson, “Neutron Tomography of Lithium (Li) Coolant inside a Niobium (Nb) Heat Pipe, *Journal of Heat Transfer*-Photogallery, Vol.136, No. 8, August 2014 (accepted for publication).
18. E. Kirchoff, K. D. Kihm, J. Rosenfeld, S. Rawal, H. Bilheux, L. Walker, S. Voisin, D. Pratt, and A. Swanson, “Neutron Tomography of Lithium (Li) Menisci inside a Molybdenum (Mo) Heat Pipe, *Journal of Heat Transfer*-Photogallery, Vol. 135, No. 8, 080902, August [1]2013.

19. K. D. Kihm, D. S. Hussey, D. M. Pratt and A. D. Swanson, “Neutron Imaging of Progressive Mixing of H_2O and D_2O inside a Metal (Al) Container,” *Journal of Heat Transfer*-Photogallery, Vol. 134, No. 8, 080904-1, August 2012.

Vita

Brad Hight was born in Knoxville, Tennessee on November 29, 1988 to Paul and Dolores Hight. He lived in Oak Ridge, Tennessee until 2007 where he attended public schooling, graduating from Oak Ridge High School in 2007. He was accepted and enrolled into the University of Tennessee, Knoxville's undergraduate department of Mechanical Engineering during the Fall of 2007. He graduated summa cum laude with a Bachelor of Science degree in Mechanical Engineering in December 2011. In the Fall of 2012, he enrolled in the Master of Science program at the University of Tennessee, Knoxville majoring in Mechanical Engineering with a concentration in thermal and fluid sciences. He joined the Micro/Nano Scale Fluidics and Energy Transport Laboratory as a graduate research assistant under the guidance of Dr. Kenneth Kihm. His graduate research focused on neutron imaging of high temperature heat pipes.